

ENHANCED DENSE CONVOLUTIONAL NETWORK FOR BRAIN TUMOR CLASSIFICATION USING MODIFIED BIRCH SEGMENTATION

CHIRANJEEVI K¹, VICTO SUDHA GEORGE G²

¹Research Scholar, Dr MGR Educational and Research Institute, Department of Computer Science and Engineering, Maduravoyal, Chennai, Tamilnadu, 600095, India.

²Professor, Dr MGR Educational and Research Institute Department of Computer Science and Engineering, Maduravoyal, Chennai, Tamilnadu, 600095, India.

Email: ¹chiru.srkr@gmail.com, victosudhageorge@drmgrdu.ac.in

ABSTRACT

The ability and experience of a radiologist is essential for the long and challenging process for detecting brain tumors. With the increasing number of patients, the number of data is maximized, making the fastest processes more expensive and inefficient. Many researchers have looked at many faster, more accurate methods to identify brain tumor classifications. In particular, Deep Learning techniques are detected to create automated systems that can achieve proper identification or segmentation of brain tumors in a shorter period of time. This article suggests a classification of four stages of brain tumors based on Edenet. The specified images are processed in the first stage using GF, and the pre-processed images are segmented using modified birch segmentation in the second stage. After segmentation, features such as shape functions (moments, area, scopes, epsilons, convex) are extracted as a third stage as new variants of texture functions (improvements in LGTP), MBP, and residual functions. In the final phase of the specified model, Edenet-based classification is performed for the classification of brain tumors, and its performance is verified using traditional methods in terms of various performance measurements.

Keywords: *Brain Tumor, Dl, Birch, Edensenet, Iltip*

1. INTRODUCTION

Brain tumors arise from abnormal brain cell proliferation due to disruptions in the brain's regulatory mechanisms [12] [15]. These tumors are primarily classified as either malignant or benign, depending on their nature. The early detection and classification of brain tumors play a crucial role in medical imaging, as they aid in determining the most effective treatment strategies to improve patient outcomes. Brain tumors can be categorized in multiple ways [18], with one common method distinguishing between malignant and other tumors.

Benign brain tumors typically develop in the skull but are not directly connected to brain tissue [9]. Meningiomas are a notable example within this category. While benign brain tumors are generally less aggressive, they can sometimes lead to life-threatening complications, unlike benign tumors in other parts of the body. In rare cases, certain benign tumors may transform into malignant ones. However, generally they do not invade by the side of brain tissue, surgical removal is often a viable and effective treatment option [13]. Malignant tumor cells are abnormal cells that divide

uncontrollably and unpredictably [10] [16]. These tumors can exert pressure on, invade, or destroy healthy brain tissue. A metastatic brain tumor refers to a tumor that has spread to the brain from another part of the body, commonly originating from the prostate, colon, breast, lung, skin, or stomach. Gliomas are the most prevalent type of malignant brain tumor [12]. These tumors consist of rapidly proliferating cells and are responsible for the majority of brain cancers. While they grow aggressively and can invade surrounding healthy tissue, they rarely spread to the nerve roots or other organs in the body. MRI is a highly effective imaging technique for detecting brain tumors without requiring surgical intervention [11] [14]. This noninvasive procedure generates high-resolution images of tumors without causing discomfort. Researchers are actively developing automated methods for brain tumor detection, with many existing systems leveraging machine learning (ML) approaches, including both supervised and unsupervised learning techniques [18].

Supervised learning methods rely on pre-trained models using labeled datasets and require additional class information. Classifying brain

tumors by identifying similarities in MRI scans can be time-consuming and labor-intensive, particularly when dealing with large datasets. To address these challenges, research suggests utilizing deep learning (DL) techniques to improve brain tumor classification [15] [19]. Deep convolutional neural networks (CNNs) have gained significant attention in image classification tasks. Various CNN techniques are applied to segment tumors in MRI scans. However, one key limitation of CNN-based techniques is that they classify images based on individual pixels, without fully considering local pixel dependencies. To overcome this limitation, manually engineered features—such as texture features derived from histograms—serve as robust descriptors for capturing local pixel dependencies [17] [20].

In this article, we propose a four-step classification approach for brain tumors based on EDenseNet, with the following key contributions:

1. After GF-based preprocessing of the input image, segmentation is performed using a modified BIRCH algorithm, as accurate segmentation plays a crucial role in precise classification.
2. We introduce an enhanced variant of the LGTP feature extraction from the segmented image, along with additional features. The extracted features are then used to train the EDenseNet-based classification model.

The structure of this research is as follows: Section 1 presents the introduction. Section 2 provides an overview of traditional methods. Section 3 details the EDenseNet model. Section 4 analyzes the EDenseNet approach, and Section 5 concludes the study.

2. LITERATURE REVIEW

In 2021, Irmak E [1] suggested CNN-based classification of brain tumors aims to facilitate early detection. Three distinct CNN algorithms were proposed for three separate classification tasks. To optimize the process, the GSO approach was employed to automatically determine the critical hyperparameters of each CNN algorithm. The proposed CNN model can assist doctors and radiologists in validating initial screenings and accurately classifying different types of brain tumors.

In 2021, Kumar R.L *et al.* [2] suggested A deep network algorithm was developed to tackle the vanishing gradient and overfitting issues by incorporating the global average pooling model along with ResNet-50. To evaluate the proposed model correctness, a simulation was conducted using 3,064 brain MRI scans featuring three types of tumors. The performance of the proposed model was compared with competing models using key performance metrics.

In 2021, Kokkalla *Set al.* [3] presented A three-class deep dense Inception ResNet model was proposed for brain tumor classification. The model integrated a deep dense architecture with a softmax layer applied to the output of the Inception ResNet v2 layer. The inclusion of the deep dense model significantly improved classification accuracy. To evaluate the proposed framework, a publicly available dataset of 3,064 brain tumor images was used, with key performance metrics applied for assessment. Additionally, the model demonstrated robust performance even when tested with noisy data.

In 2021, Alhassan and Zainon [4] A system was proposed for the automatic classification of various types of brain tumors. The process began with the acquisition of brain images using a T1-weighted contrast-enhanced MRI dataset. To enhance visibility, the raw images underwent normalization before feature extraction. The Histogram of Oriented Gradients (HOG) method was then applied to extract feature vectors from the normalized images. Among various feature descriptors, the histogram descriptor effectively captured edge and contour details. Finally, a CNN model was employed to classify gliomas, pituitary tumors, and meningiomas using the extracted features as input.

In 2021, Rao and Karunakara K. [5] suggested A detailed analysis was carried out on MRI-based brain tumor classification and segmentation. The proposed model first described essential MRI preprocessing steps, including image registration, bias field correction, and non-brain tissue removal. Furthermore, the study examined the incorporation of MRI-assisted brain tumor classification into routine clinical practice. Additionally, an assessment of the algorithm's current performance was provided.

In 2020, Begum S.S. and Lakshmi [6] suggested A method was developed for precise brain tumor detection by integrating recurrent neural networks

(RNN) with optimal wavelet-based statistical texture features. The process began with noise reduction as the initial step in preprocessing brain MRI scans. Once noise-free, the images were used for texture feature extraction. To enhance efficiency, the Optimal Grey Wolf Optimization (OGSA) technique used to reduce the count of extracted features. Finally, a collected subset of features was fed into an RNN classifier to determine whether an image was normal or pathological.

In 2021, Novak *et al.* [7] introduced A novel classifier, DeepSurvNet, incorporating deep CNN, was proposed to accurately categorize tumor patients into four survival groups based on histological images. The proposed model achieved high precision during testing on the specified datasets using DeepSurvNet. The results demonstrated for predicting the survival rate of brain cancer patients using histopathology images that DeepSurvNet is a reliable classifier.

In 2021, Al-qazzaz *et al.* [8] employed A hybrid approach combining handcrafted and CNN-assisted features was developed for the automated segmentation of brain tumor tissue. To address the limitations of the CIFAR network, CNN-assisted features were extracted and integrated with histogram-based textural characteristics. These features, along with pixel intensity values from the original MRI scans, were then fed into a decision tree (DT) classifier to categorize voxels within MRI images into different tumor tissue types.

2.1 Review

Various research scientists strive to identify challenges that must be addressed to effectively manage brain tumor patients and enhance our understanding and treatment capabilities. The following are key difficulties encountered in the reviewed studies (Table I): In Deep CNN [1], refining the intensity adjustment process was crucial to optimizing segmentation effectiveness. In ResNet-50 [2], the proposed models computation time must be reduced. This was a primary focus. Deep Dense Inception ResNet [3] did not emphasize reducing computational time or parameter count without compromising performance. Hard Swish-assisted ReLU-CNN [4] required a clustering-based segmentation method to improve brain tumor classification accuracy. The development of an automated, medically applicable approach [5] for glioma segmentation was necessary to support critical prognosis. OGSA [6]

posed challenges in identifying tumor type, as well as determining the tumor's thickness, size, and precise location. In DeepSurvNet [7], the processing time needed to be carefully considered. In CIFAR [8], initializing the network and establishing an ideal case was essential. These challenges highlight the ongoing need for advancements in brain tumor analysis and segmentation techniques.

3. EDENSENET-BASED BRAIN TUMOR CLASSIFICATION

The brain is one of the most vital organs in the human body, with new features being discovered every day. It has been the focus of numerous studies in the literature. Various deep learning-based medical image analysis techniques have been developed for diagnosing and monitoring brain health using MRI data. In this study, we propose a four-step brain tumor classification approach based on EDenseNet, which includes preprocessing, segmentation, feature extraction, and classification. The proposed EDenseNet-based brain tumor classification model is depicted in Fig. 1.

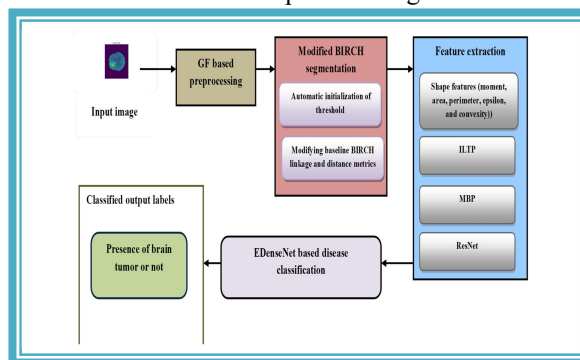


Fig 1: Proposed EDenseNet-based brain tumour classification model general structure

3.1 Image preprocessing:

As the first step in image processing, the image denoising technique aims to reduce artifacts in image collection and normalize images across the dataset. This research employs a linear smoothing filter known as GF [21], which determines its weights based on the properties of a Gaussian function. This filter is highly effective in eliminating noise originating from a normal distribution. Equation (1) defines the zero-mean Gaussian function in a single dimension, representing the Gaussian spread parameter.

$$G(x) = e^{-\frac{x^2}{2\sigma^2}} \tag{1}$$

3.2 Modified BIRCH segmentation:

Segmenting a brain tumor involves distinguishing it from healthy brain tissue, providing valuable insights for diagnosis and treatment planning in clinical settings. However, due to the irregular shape and indistinct boundaries of tumors, this remains a challenging task. In this research, the next step in image preprocessing utilizes a modified BIRCH segmentation technique. The modified BIRCH segmentation model is illustrated in Fig. 2. The segmentation process consists of two key phases:

Automatic initialization of threshold *th* (modified)

- Modifying baseline BIRCH linkage and distance metrics (modified)

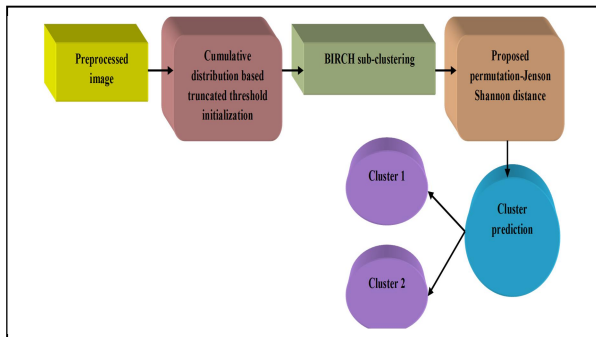


Fig. 2 Modified Birch Segmentation Model

3.2.1 Automatic initialization of threshold:

The modified BIRCH technique [22] constructs a CF-tree, where each submission in a leaf node must meet a specific threshold. Traditional methods use a static threshold, often leading to low-quality clusters, as it follows a matching grouping strategy for any given dataset. This research aims to enhance clustering accuracy by dynamically initializing the threshold value in the CF-entry. Consequently, the most recent threshold adjustments are stored in the CF-Leaf parameter. While the CF-Leaf utilizes an additional parameter, the CF-Node continues to follow the original equation.

Using the conventional BIRCH algorithm, a data point is assigned to a CF-node based on the closest distance estimation. If the leaf radius remains

within the threshold, the data point is incorporated into the CF-leaf. However, if it exceeds the threshold, new leaves are created. If the value surpasses the leaf limit, a split parent is generated. In contrast, the modified BIRCH algorithm immediately initializes a new data point exceeding the threshold. To reduce parent splits in BIRCH, the leaf radius scale is expanded. Conventionally, the threshold is set to 0.1. In the proposed approach, a cumulative distribution-based truncated threshold is calculated, as shown in Eq. (2), where the input image parameters are incorporated. The threshold for the proposed calculation is determined in Eq. (3).

$$Scdt(x, y) = \begin{cases} th; & \text{if } src(x, y) > th \\ src(x, y); & \text{otherwise} \end{cases} \tag{2}$$

$$th = \frac{1}{2} + \left(\frac{1}{\pi}\right) \cdot \arctan\left(\frac{x - \theta}{\lambda}\right) \tag{3}$$

3.2.2 Modifying baseline BIRCH linkage and distance metrics:

In this section, we introduce the linkage techniques and distance metrics employed in our experiments to evaluate the modified BIRCH algorithm. The goal is to achieve an optimal balance between clustering accuracy, memory usage, and computational complexity.

Linkage method:

The primary distinction between different hierarchical clustering techniques lies in the method used to measure the distance between clusters. In the agglomerative approach, for instance, data objects are progressively merged to form clusters, starting with those that are closest to each other. Various methods exist for determining the distance between two clusters, each formed from multiple data points, depending on the differences among the individual members of the clusters. The linkages used in these methods are represented by the notation below.

Through the clusters c_1 and c_2 , Cluster C is generated

- ✓ n_c refers to the object count inside the cluster C
- ✓ x_{C_i} refers to i^{th} objects within the cluster C

Distance Similarity:

Before making data-driven decisions, distance metrics are typically used to analyze the input data pattern. Accurate distance measurement plays a crucial role in classification, information processing, and various clustering processes. In this phase, we employ a proposed permutation JSD model for distance calculation, as defined in Eq. (5), where it represents the standard deviation (SD) of the image. Traditionally, this calculation is performed using Eq. (4), where it denotes clusters. Finally, a prediction is made, and each record is assigned to the appropriate cluster.

$$JSD(P, Q) = \frac{1}{2} [D(P, M) + D(Q, M)] \tag{4}$$

Where,

$$D(P, M) = \sum_{i=1}^n p_i \ln\left(\frac{p_i}{q_i}\right); M = \frac{1}{2}(P + Q),$$

$$PJSD(P, Q) = \frac{1}{2} [wf * D(P, M) + wf * D(Q, M)] \tag{5}$$

Where, $wf = \frac{1}{\sigma_i^2}$

3.3 Feature Extraction:

In this phase, various features are extracted from the segmented image, including shape features (moment, area, perimeter, epsilon, and convexity), the enhanced LGTP feature, the MBP feature, and ResNet features.

3.3.1 Improved LGTP feature:

We have achieved exceptionally high detection rates by applying Gabor filter encoding with the LTP operator [23]. This method utilizes Gabor wavelets to extract diverse information from an image. LTP is more resistant to noise and provides a more precise representation of local texture. When combined, Gabor wavelets and LTP enhance

overall performance. Our brain tumor detection system employs the LGTP approach, which remains effective under various lighting conditions. Traditionally, LGTP is computed using Eq. (6), where represents the intensity value of the neighboring pixel, denotes the intensity value of the center pixel, and indicates the number of neighboring pixels around the center pixel. In the proposed method, the improved LGTP calculation is performed using Eq. (7), which incorporates a small scaling factor.

$$LTP(x_c, y_c) = \sum_{n=0}^{p-1} K(f_n - f_c) 2^p \tag{6}$$

Where,

$$K(f_n - f_c) = \begin{cases} -1; & f_n < |f_c - S| \\ 0; & |f_c - S| < f_n < |f_c + S| \\ 1; & f_n > |f_c + S| \end{cases}$$

$$ILTP(x_c, y_c) = \sum_{n=0}^{p-1} K^*(f_n - f_c) 2^p \tag{7}$$

Where,

$$K^*(f_n - f_c) = \begin{cases} -1; & f_n < (1-\sigma)f_c \\ 0; & (1-\sigma)f_c \leq f_n \leq (1+\sigma)f_c \\ 1; & f_n > (1+\sigma)f_c < (f_c + \sigma) \end{cases}$$

3.3.2 MBP feature [24]:

Instead of consistently using the center pixel, the MBP operator thresholds pixels based on their median value within a defined region (typically 3×3). This approach enhances sensitivity to microstructures while improving noise resistance. The MBP function at a given pixel in the segmented input image is defined by Eq. (8), where represents the median value and denotes the patch size.

$$MBP(i, j) = \sum_{k=0}^{L-1} 2^k H(b_k - \tau) \quad (8)$$

3.3.3 ResNet feature Rf :

The concept of Residual Blocks was introduced to address the issue of exploding or vanishing gradients. In this design, we implement a technique called skip connections, which bypass certain layers to directly link activations to subsequent layers. This forms residual blocks, which are then stacked to construct ResNet. Each ResNet layer consists of two key components: a residual module and a skip connection. These layers are composed of multiple convolutional layers, collectively referred to as residual blocks. For a given input, the block outcome is recursively determined using Eq. (9) which incorporates convolution sequences, batch normalization, and the ReLU activation function (nonlinearity). Additionally, each layer is defined using Eq. (10), where W_i represents the weight matrix and B denotes batch normalization.

$$y_i = f_i(y_{i-1}) + y_{i-1} \quad (9)$$

$$f_i(x) = W_i^{(1)} * \sigma(B(W_i^{(2)} * \sigma(B(x)))) \quad (10)$$

Finally, the features that were extracted from the input segmented image are indicated as:

$$F = [S_p \ ILTP \ MBP \ Rf]$$

3.4 EDenseNet-based classification:

At this stage, the final output classes (presence or absence of a brain tumor) are determined by feeding the extracted features into EDenseNet [25]. EDenseNet shares many similarities with the widely known ResNet, as both utilize skip connections to improve computational efficiency while preserving network depth. However, unlike ResNet, where block outputs and inputs are combined through addition, EDenseNet concatenates the layer input with the output of the previous layer.

In a dense block, all layers receives inputs from their previous layers and submits outputs to all next layers. This approach effectively mitigates the vanishing gradient issue commonly encountered in deep neural networks (DNNs) by regulating network depth through skip connections. Convolutional Neural Networks (CNNs) enable the representation of connections over two layers, as

expressed in Eq. (11), which defines a composite function consisting of batch normalization, ReLU, and pooling operations. Figures 3 and 4 illustrate the traditional DenseNet and EDenseNet representations, respectively.

$$x_l = H(x_{l-1})$$

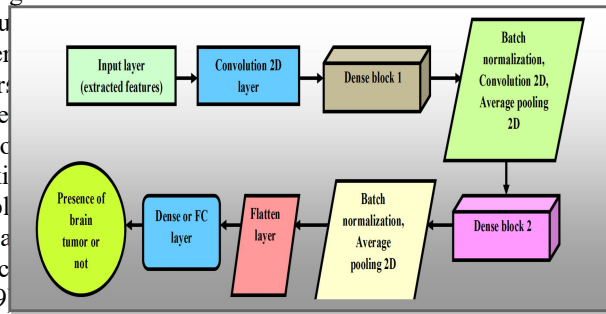


Fig 3: Traditional Densenet Representation

In a CNN, each successive layer receives the feature maps generated by the previous layer as input. Conversely, in a ResNet block with a skip connection, the relationship between two layers can be described using Eq. (12). Within the residual block, the feature maps produced by one layer are combined with the layer's input and then passed to the next layer. In contrast, the connection between layers within the dense blocks of conventional DenseNet or EDenseNet is represented by Eq. (13), which defines the output concatenation generated across layers. In a dense block, this concatenated output is forwarded to the next layer, meaning each layer receives as input the combined information from all preceding layers. These networks are termed EDenseNet due to their highly interconnected structure.

$$x_l = H(x_{l-1}) + x_{l-1} \quad (12)$$

$$F_l = H(F_0, F_1, \dots, F_{l-1}) \quad (13)$$

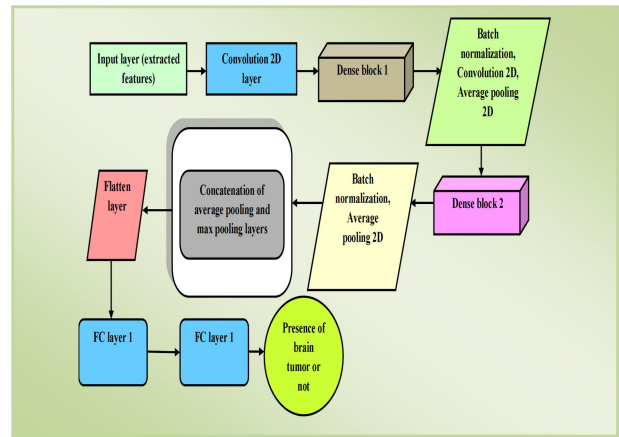


Fig 4: Edensenet Representation

EDenseNet incorporates a global average pooling and global max pooling concatenation as a transition step to connect the convolution layer output with the fully connected (FC) layer input. This operation is mathematically represented in Eq. (14), where denotes the output of the convolution layers, and represents the concatenated result, which serves as the input to the FC layer. By combining these two pooling operations, the network can leverage both methods and select the most effective one for a given scenario.

Additionally, EDenseNet employs two FC layers with a dropout value of 0.5 instead of a single FC layer. The EDenseNet FC structure includes dropout (0.5), batch normalization, ReLU activation, and an FC layer, followed by another batch normalization set, dropout, and an additional FC layer. Finally, the network applies a logarithmic Softmax function. The FC layers are defined in Eq. (15), where represents the number of output classes, denotes the concatenated pooling layer output, and corresponds to the two FC layers incorporating the Softmax function.

$$y = \text{Con}(M(x), A(x))$$

(14)

$$c = F(y)$$

(15)

4. RESULT ANALYSIS ON EDENSENET FOR BRAIN TUMOR CLASSIFICATION

4.1 Simulation Procedure

The proposed brain tumor classification was implemented using Python, with the system configuration detailed in Table II. Additionally, the BRaTS 2021 Task 1 Dataset was sourced from [26]. To validate the accuracy of EDenseNet in brain tumor classification, it was compared with conventional methodologies, including NN, GRU, LSTM, DEEP-CNN [1], DBN, RNGAP [2], and SVM. The evaluation was conducted based on various metrics, such as precision, false positive rate (FPR), and accuracy. Moreover, segmentation performance and statistical analysis were carried out. Sample images, conventional segmentation results, and Modified BIRCH-segmented images are presented in Fig. 5.

Table II: System Configuration

Device Specification	
Processor	11th Gen Intel(IR) Core (TM) i5-1135G7 @ 2.40GHz 2.42 GHz
Installed RAM	16.0 GB (15.7 GB usable)
Software Specification	
PYTHON version	Python 3.7.9

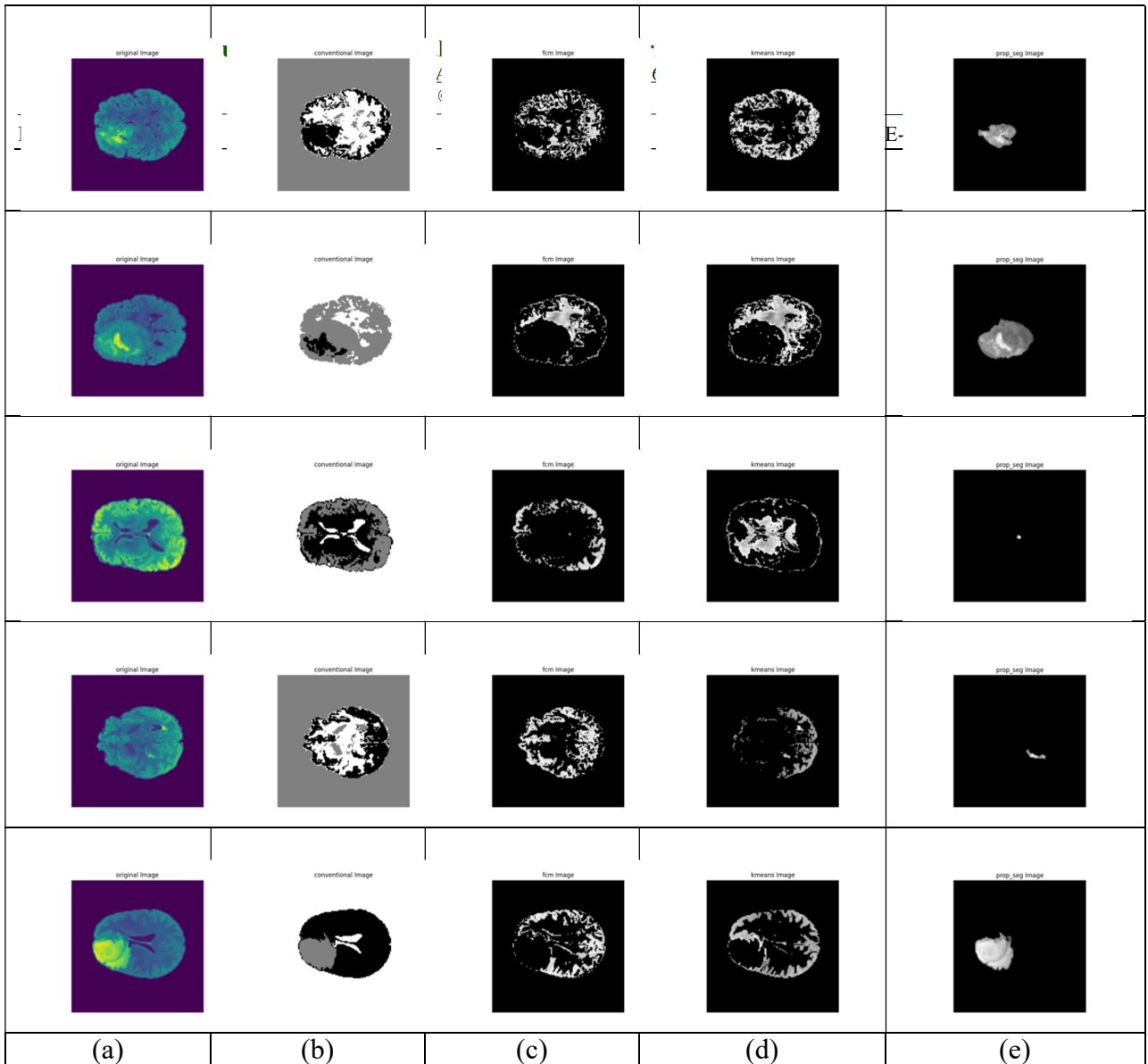


Fig 5 Images For Brain Tumor Segmentation

A) Original Image B) Conventional BIRCH Segmented Image C) FCM Segmented Image
D) K-Means Segmented Image And E) Modified BIRCH Segmented Image

4.2 Brats 2021 Task 1 Dataset Description

For this year's BraTS challenge, a large collection of multi-institutional, clinically acquired multi-parametric MRI (mpMRI) scans of glioma, with pathologically confirmed diagnoses and available MGMT promoter methylation status, is used for training, testing, and validation. The datasets for this year's challenge have been enhanced from BraTS'20, incorporating a greater number of clinically acquired mpMRI scans, particularly for Task 1. To ensure an objective evaluation of tumor segmentations, ground truth annotations of tumor sub-regions are generated and verified by expert neuroradiologists for each subject included in the training, validation, and testing datasets.

4.3 Assessment On Edensenet And Traditional Methods For Brain Tumour Classification Regarding Positive Metric

Figure 6 illustrates the positive metric assessment of EDenseNet compared to NN, GRU, LSTM, DEEP-CNN, DBN, RNGAP, and SVM for brain tumor classification. Additionally, the model's performance is evaluated while varying the training rate from 60% to 90%. Achieving higher positive metric scores is essential for accurately classifying brain tumors. As shown in Figure 6(a), at a 90% training rate, EDenseNet achieves a specificity of 0.9206, whereas NN, GRU, LSTM, DEEP-CNN, DBN, and SVM obtain values of 0.8412, 0.9047, 0.8412, 0.8889, 0.9206, and 0.8730, respectively. Furthermore, EDenseNet demonstrates higher

sensitivity than the other methods across all training percentages.

As shown in Figure 6(b), the accuracy of EDenseNet steadily increased as the training rate improved. Notably, at a training rate of 80%, EDenseNet achieved the highest accuracy of 0.9521, outperforming NN, GRU, LSTM, DEEP-CNN, DBN, RNGAP, and SVM, which recorded lower accuracy values. Similarly, EDenseNet attained the highest specificity of 0.9560 at a training rate of 70%, while NN (0.8956), GRU (0.8626), LSTM (0.8736), DEEP-CNN (0.8956), DBN (0.8791), RNGAP (0.8736), and SVM (0.8626) exhibited lower specificity scores. These findings demonstrate that the EDenseNet algorithm delivers exceptional performance, confirming its effectiveness in brain tumor classification. This improvement is attributed to enhancements in the feature extraction and classification phases.

4.4 Assessment On Edensenet And Traditional Methods For Brain Tumour Classification Regarding Negative Metric

Figure 7 presents a comparison of the negative metric evaluation of EDenseNet against NN, GRU, LSTM, DEEP-CNN, DBN, RNGAP, and SVM for brain tumor segmentation. For accurate classification, it is essential to minimize both the False Negative Rate (FNR) and False Positive Rate (FPR). At a training rate of 90%, EDenseNet achieves an FNR of 0.0158, whereas NN, GRU, LSTM, DEEP-CNN, RNGAP, and SVM exhibit higher FNR values of 0.1746, 0.0793, 0.1587, 0.1428, 0.1746, and 0.1269, respectively. Additionally, at a training rate of 70%, EDenseNet attains the lowest FPR of 0.0439, outperforming NN, GRU, LSTM, DEEP-CNN, DBN, RNGAP, and SVM, which record higher FPR values. These results highlight EDenseNet's superior capability in brain tumor classification, attributed to the enhanced LGTP-based feature extraction process.

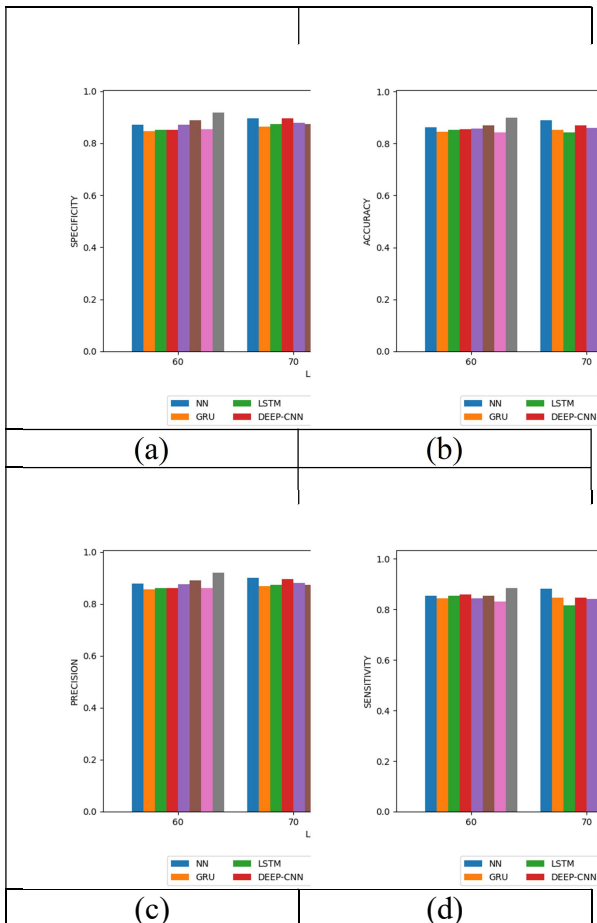


Fig 6 Validation On Edensenet And Conventional Schemes With Regard To Positive Metric For Brain Tumour Classification

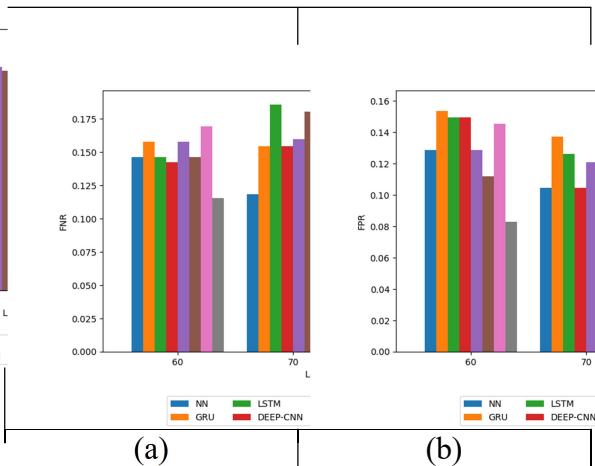


Fig 7 Validation On Edensenet And Conventional Schemes With Regard To Negative Metric For Brain Tumour Classification

4.5 Assessment On Edensenet And Traditional Methods For Brain Tumour Classification Regarding Other Metrics

Figure 8 illustrates the evaluation of additional performance metrics for EDenseNet compared to traditional methods in brain tumor classification. The model's performance is assessed against NN, GRU, LSTM, DEEP-CNN, DBN, RNGAP, and SVM. At a training rate of 70%, EDenseNet achieves an F-measure of 0.9587, indicating precise brain tumor classification, while NN, GRU, LSTM, DEEP-CNN, DBN, SVM, and RNGAP exhibit lower F-measure values.

Additionally, at a 90% training rate, EDenseNet attains a Matthews Correlation Coefficient (MCC) of 0.9065, outperforming NN (0.6667), GRU (0.8255), LSTM (0.6825), DEEP-CNN (0.7464), DBN (0.7793), RNGAP (0.7157), and SVM (0.7460). Similarly, at an 80% training rate, EDenseNet achieves the highest Negative Predictive Value (NPV) of 0.9833, surpassing all other models. The implementation of an enhanced segmentation approach has led to a more effective feature extraction strategy, contributing to superior performance across these additional metrics.

measures, where higher accuracy values are essential for precise tumor classification. EDenseNet consistently outperforms the other models, yielding superior classification results. Specifically, under the median statistical metric, EDenseNet achieves the highest accuracy of 0.9523, while NN (0.8753), GRU (0.8611), LSTM (0.8477), DEEP-CNN (0.8711), DBN (0.8618), RNGAP (0.8628), and SVM (0.8492) exhibit lower accuracy rates. Additionally, EDenseNet records the highest accuracy under the maximum statistical metric, significantly surpassing all other methods. Overall, EDenseNet demonstrates improved performance across all statistical metrics, reinforcing its effectiveness in accurately classifying brain tumors.

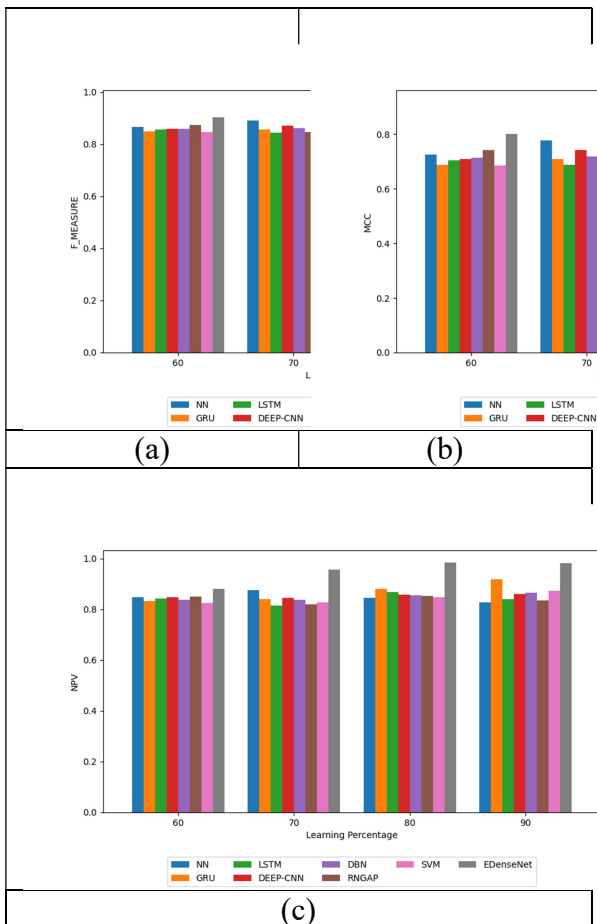


Fig 8 Validation On Edensenet And Conventional Schemes With Regard To Other Metrics For Brain Tumour Classification

4.6 Statistical Evaluation On Edensenet And Conventional Methods For Brain Tumour Classification Regarding Accuracy Measure

Table III presents the statistical evaluation of EDenseNet in comparison to NN, GRU, LSTM, DEEP-CNN, DBN, RNGAP, and SVM for brain tumor classification. The analysis is conducted using the accuracy metric across various statistical

Table III: Statistical Study On Edensenet And Traditional Approaches With Regard To Accuracy For Brain Tumour Classification

Statistical metrics	NN	GRU	LSTM	DEEP-CNN	DBN	RNGAP	SVM	EDenseNet
Mean	0.8701	0.8698	0.8523	0.8674	0.8672	0.8604	0.8534	0.9406
Minimum	0.8333	0.8443	0.8413	0.8543	0.8563	0.8457	0.8423	0.9002
Standard Deviation	0.0247	0.0262	0.0124	0.0077	0.0129	0.0099	0.0119	0.0234
Maximum	0.8964	0.9127	0.8725	0.8730	0.8898	0.8703	0.8730	0.9574
Median	0.8753	0.8611	0.8477	0.8711	0.8618	0.8628	0.8492	0.9523

4.7 Segmentation Performance Analysis On Modified BIRCH And The Conventional Schemes For Brain Tumour Segmentation Regarding Dice Coefficient, Jaccard Coefficient And Segmentation Accuracy

Table IV presents the segmentation performance evaluation of the Modified BIRCH algorithm compared to FCM, K-means, and Conventional BIRCH for brain tumor segmentation. The assessment is based on the Jaccard coefficient, Dice coefficient, and

segmentation accuracy. The results indicate that the Modified BIRCH algorithm achieves superior segmentation performance. Specifically, in terms of segmentation accuracy, Modified BIRCH attains the highest value of 89.5671, outperforming FCM (67.3173), K-means (55.1679), and Conventional BIRCH (61.2671). Likewise, the Modified BIRCH method records the highest values for both the Jaccard and Dice coefficients compared to the traditional approaches. These findings highlight the effectiveness of the Modified BIRCH segmentation approach, demonstrating its improved accuracy and robustness in brain tumor segmentation.

Table IV: Segmentation Performance Examination On Modified BIRCH And The Traditional Methodologies In Terms Of Jaccard Coefficient, Dice Coefficient And Segmentation Accuracy For Brain Tumour Segmentation

Methods	FCM	K-means	Conventional BIRCH	Modified BIRCH
Jaccard Coefficient	60.8371	57.0977	67.2216	86.4921
Segmentation Accuracy	67.3173	55.1679	61.2671	89.5671
Dice Coefficient	67.6688	56.7351	59.0165	86.6136

5. CONCLUSION

In this article, we proposed a four-stage classification framework for brain tumors using EDenseNet. In the first stage, the input image underwent preprocessing using a Gabor Filter (GF). In the second stage, the preprocessed image was segmented using the Modified BIRCH segmentation approach. The third stage involved feature extraction from the segmented image, including shape features (moment, area, perimeter, epsilon, and convexity), Improved LGTP, MBP, and ResNet features. Finally, in the fourth stage, EDenseNet was utilized for classification by feeding the extracted features into the network to predict the output labels. Performance evaluation demonstrated the superiority of the proposed model over conventional methods, achieving 89.5% segmentation accuracy, thereby enhancing classification precision.

REFERENCES

[1] Irmak, E. Multi-Classification of Brain Tumor MRI Images Using Deep Convolutional Neural Network with Fully Optimized Framework. Iran J Sci Technol Trans Electr Eng 45, 1015–

1036 (2021). <https://doi.org/10.1007/s40998-021-00426-9>

- [2] Kumar, R.L., Kakarla, J., Isunuri, B.V., & Munesh Singh, "Multi-class brain tumor classification using residual network and global average pooling", *Multimed Tools Appl.*, vol. 80, pp. 13429–13438, 2021. <https://doi.org/10.1007/s11042-020-10335-4>
- [3] Kokkalla, S., Kakarla, J., Venkateswarlu, I.B., & Munesh Singh, "Three-class tumor classification using deep dense inception residual network", *Soft Comput.*, vol. 25, pp. 8721–8729, 2021. <https://doi.org/10.1007/s00500-021-05748-8>
- [4] Alhassan, A.M., & Zainon, W.M.N.W., "Brain tumor classification in magnetic resonance image using hard swish-based RELU activation function-convolutional neural network", *Neural Comput & Applic.*, vol. 33, pp. 9075–9087, 2021. <https://doi.org/10.1007/s00521-020-05671-3>
- [5] Rao, C.S., & Karunakara, K., "A comprehensive review on brain tumor segmentation and classification of MRI images", *Multimed Tools Appl.*, vol. 80, pp. 17611–17643, 2021. <https://doi.org/10.1007/s11042-020-10443-1>
- [6] Begum, S.S., & Lakshmi, D.R., "Combining optimal wavelet statistical texture and recurrent neural network for tumour detection and classification over MRI", *Multimed Tools Appl.*, vol. 79, pp. 14009–14030, 2020. <https://doi.org/10.1007/s11042-020-08643-w>
- [7] Zadeh Shirazi, A., Fornaciari, E., Bagherian, N.S., Lisa M. Ebert, Barbara Koszyca & Guillermo A. Gomez, "DeepSurvNet: deep survival convolutional network for brain cancer survival rate classification based on histopathological images", *Med Biol Eng Comput.*, vol. 58, pp. 1031–1045, 2020. <https://doi.org/10.1007/s11517-020-02147-3>
- [8] Al-qazzaz, S., Sun, X., Yang, H., Yingxia Yang, Ronghua Xu, Len Nokes & Xin Yang, "Image classification-based brain tumour tissue segmentation", *Multimed Tools Appl.*, vol. 80, pp. 993–1008, 2021. <https://doi.org/10.1007/s11042-020-09661-4>
- [9] Devunooru, S., Alsadoon, A., Chandana, P.W.C., & Azam Beg, "Deep learning neural

- networks for medical image segmentation of brain tumours for diagnosis: a recent review and taxonomy”, *J Ambient Intell Human Comput*, vol. 12, pp. 455–483, 2021. <https://doi.org/10.1007/s12652-020-01998-w>
- [10] Koyuncu, H., Barstuğan, M. & Ozic, M.U., “A comprehensive study of brain tumour discrimination using phase combinations, feature rankings, and hybridised classifiers”, *Med Biol Eng Comput*, vol. 58, pp. 2971–2987, 2020. <https://doi.org/10.1007/s11517-020-02273-y>
- [11] Jalali, V., Kaur, D., “A study of classification and feature extraction techniques for brain tumor detection”, *Int J Multimed Info Retr*, vol. 9, pp. 271–290, 2020. <https://doi.org/10.1007/s13735-020-00199-7>
- [12] Sethy, P.K., Behera, S.K., “A data constrained approach for brain tumour detection using fused deep features and SVM”, *Multimed Tools Appl*, vol. 80, pp. 28745–28760, 2021. <https://doi.org/10.1007/s11042-021-11098-2>
- [13] Polat, O., & Güngen, C., “Classification of brain tumors from MR images using deep transfer learning”, *J Supercomput*, vol. 77, pp. 7236–7252, 2021. <https://doi.org/10.1007/s11227-020-03572-9>
- [14] Ayadi, W., Elhamzi, W., Charfi, I., & Mohamed Atri, “Deep CNN for Brain Tumor Classification”, *Neural Process Lett.*, vol. 53, pp. 671–700, 2021. <https://doi.org/10.1007/s11063-020-10398-2>
- [15] Rehman, A., Naz, S., Razzak, M.I., Faiza Akram & Muhammad Imran, “A Deep Learning-Based Framework for Automatic Brain Tumors Classification Using Transfer Learning”, *Circuits Syst Signal Process*, vol. 39, pp. 757–775, 2020. <https://doi.org/10.1007/s00034-019-01246-3>
- [16] Karunamuni, R., Tringale, K.R., Burkeen, J., Michelle D. Tibbs, Minh-Phuong Huynh-Le, Naeim Bahrami, Deborah Marshall, Tyler M. Seibert, Carrie R. McDonald & Jona A. Hattangadi-Gluth, “Multi-domain neurocognitive classification of primary brain tumor patients prior to radiotherapy on a prospective clinical trial”, *J Neurooncol*, vol. 146, pp. 131–138, 2020. <https://doi.org/10.1007/s11060-019-03353-2>
- [17] Shrot, S., Salhov, M., Dvorski, N., Eli Konen, Amir Averbuch & Chen Hoffmann, “Application of MR morphologic, diffusion tensor, and perfusion imaging in the classification of brain tumors using machine learning scheme”, *Neuroradiology*, vol. 61, pp. 757–765, 2019. <https://doi.org/10.1007/s00234-019-02195-z>
- [18] Narmatha, C., Eljack, S.M., Tuka, A.A.R.M., S. Manimurugan & Mohammed Mustafa, “A hybrid fuzzy brain-storm optimization algorithm for the classification of brain tumor MRI images”, *J Ambient Intell Human Comput*, 2020. <https://doi.org/10.1007/s12652-020-02470-5>
- [19] Dandu, J.R., Thiyagarajan, A.P., Murugan, P.R., & Vishnuvarthanan Govindaraj, “Brain and pancreatic tumor segmentation using SRM and BPNN classification”, *Health Technol.*, vol. 10, pp. 187–195, 2020. <https://doi.org/10.1007/s12553-018-00284-2>
- [20] Mishra, S., Sahu, P. & Senapati, “M.R. MASCA–PSO based LLRBFNN model and improved fast and robust FCM algorithm for detection and classification of brain tumor from MR image”, *Evol. Intel.*, vol. 12, pp. 647–663, 2019. <https://doi.org/10.1007/s12065-019-00266-x>
- [21] Madhuri Pawar and Dr. Deepali Sale, “MRI and CT Image Denoising using Gaussian Filter, Wavelet Transform and Curvelet Transform”, *International Journal of Engineering Science and Computing*, Volume 7, May 2017.
- [22] Maysarah Mohammad Barham, “An Improved BIRCH Algorithm for Breast Cancer Clustering”, MEU, 2020
- [23] Madasamy Raja, G. and V. Sadasivam, “Optimized Local Ternary Patterns: A New Texture Model with Set of Optimal Patterns for Texture Analysis”, *Journal of Computer Science* 9 (1): 1-15, 2013
- [24] Adel Hafiane, Kannappan Palaniappan, Guna Seetharaman, “Adaptive Median Binary Patterns for Texture Classification”, 2014 22nd International Conference on Pattern Recognition



[25] Ritika Dhiman & Gurkanwal Singh Kang & Varun Gupta, "Modified dense convolutional networks based emotion detection from speech using its paralinguistic features", Multimedia Tools and Applications, <https://doi.org/10.1007/s11042-021-11210-6>

[26]<https://www.kaggle.com/datasets/dschettler8845/brats-2021-task1>

Nomenclature

Abbreviation	Description
MRI	Magnetic Resonance Imaging
ML	Machine Learning
DL	Deep Learning
CNN	Convolutional Neural Network
ResNet	Residual Network
RNN	Recurrent Neural Network
OGSA	Oppositional Gravitational Search Algorithm
DeepSurvNet	Deep Survival Convolutional Network
GSO	Grid Search Optimization
HOG	Histogram of Oriented Gradients
DT	Decision Tree
DNN	Deep Neural Network
GF	Gaussian Filtering
BIRCH	Balanced Iterative Reducing and Clustering Using Hierarchies
JSD	Jensen-Shannon Divergence
SD	Standard Deviation
CF	Clustering Feature
LGTP	Local Gabor Ternary Pattern
MBP	Median Binary Pattern
LTP	Local Ternary Patterns
ReLU	Rectified Linear Units
FC	Fully Connected
NN	Neural Network
GRU	Gated Recurrent Unit
LSTM	Long Short-Term Memory
DBN	Deep Belief Network
SVM	Support Vector Machine
RNGAP	Residual Network and Global Average Pooling

		abstractions from real images.	time or parameter count without compromising performance.
Alhassan, A.M., & Zainon, W.M.N.W., [4]	Hard Swish assisted ReLU-CNN	It effectively selects the relevant feature vectors from the extracted features.	The proposed approach requires a clustering-based segmentation method to enhance the accuracy of brain tumor classification.
Rao, C.S., & Karunakara, K. [5]	CNN, DNN	DNN possesses enhanced self-learning capabilities.	It is essential to promote the development of an automated, medically applicable approach for glioma segmentation to aid in critical prognosis.
Begum, S.S., & Lakshmi, D.R. [6]	OGSA	It achieved flawless accuracy.	Identifying the tumor type and accurately determining its thickness, size, and location proved to be challenging.
Novak, J., et al [7]	DeepSurvNet	It attained high classification accuracy.	The processing time of the proposed system must be taken into account.
Al-qazzaz, et al [8]	CIFAR	It improved the overall tumor F-measure.	Initializing the network and establishing an ideal case was essential.

Table I: Pros And Cons: Conventional Techniques

Author [Citation]	Methods	Pros	Cons
Irmak, E. [1]	Deep CNN	The proposed approach achieved the highest classification accuracy, effectively segmenting brain tumor tissue	To optimize segmentation efficacy, refining the intensity adjustment process was crucial.
Kumar, R.L., et al [2]	ResNet-50	The approach achieved a high mean accuracy both with and without augmented data.	The proposed models computation time must be reduced.
Kokkalla, S., et al [3]	Deep dense inception ResNet	The model was capable of directly learning high-level	The model does not focus on reducing computational